STRUCTURAL SCIENCE CRYSTAL ENGINEERING MATERIALS

ISSN 2052-5206

Structure refinement using precession electron diffraction tomography and dynamical diffraction: tests on experimental data

Lukáš Palatinus,[a]* Cinthia Antunes Corrêa,[a,b] Gwladys Steciuk,[c] Damien Jacob,[d] Pascal Roussel,[e] Philippe Boullay,[c] Mariana Klementová,[a] Mauro Gemmi,[f] Jaromír Kopeček,[a] M. Chiara Domeneghetti,[g] Fernando Cámara[h] and Václav Petříček[a]

[a]Institute of Physics of the AS CR, Na Slovance 2, Prague, Czech Republic, [b]Department of Physics of Materials, Charles University, Ke Karlovu 5, 121 16 Prague, Czech Republic, [c]Laboratoire CRISMAT, UMR CNRS 6508, ENSICAEN, 6 Bd Maréchal Juin, F-14050 Caen CEDEX 4, France, [d]UMET, Université Lille1, CNRS UMR 8207, 59655 Villeneuve d'Ascq, France, [e]UCCS, ENSCL, CNRS UMR 8181, 59652 Villeneuve d'Ascq, France, [f]Center for Nanotechnology Innovation@NEST, Istituto Italiano di Tecnologia, Piazza S. Silvestro 12, Pisa, Italy, [g]Dipartimento di Scienze della Terra e dell'Ambiente, Università di Pavia, 27100 Pavia, Italy, and [h]Dipartimento di Scienze della Terra, Università di Torino, 10125 Torino, Italy. *Correspondence e-mail: palat@fzu.cz

Received 11 August 2015
Accepted 11 September 2015

Edited by R. Černý, University of Geneva, Switzerland

Keywords: dynamical diffraction; electron diffraction tomography; electron crystallography; precession; mayenite; kaolinite; orthopyroxene.

Supporting information: this article has supporting information at journals.iucr.org/b

The recently published method for the structure refinement from three-dimensional precession electron diffraction data using dynamical diffraction theory [Palatinus *et al.* (2015). *Acta Cryst.* A**71**, 235–244] has been applied to a set of experimental data sets from five different samples – Ni_2Si, $PrVO_3$, kaolinite, orthopyroxene and mayenite. The data were measured on different instruments and with variable precession angles. For each sample a reliable reference structure was available. A large series of tests revealed that the method provides structure models with an average error in atomic positions typically between 0.01 and 0.02 Å. The obtained structure models are significantly more accurate than models obtained by refinement using kinematical approximation for the calculation of model intensities. The method also allows a reliable determination of site occupancies and determination of absolute structure. Based on the extensive tests, an optimal set of the parameters for the method is proposed.

1. Introduction

Least-squares refinement of crystal structure parameters against diffraction data is a standard and by far the most common way of optimizing crystal structure models. This technique is mature and frequently used in combination with X-ray or neutron single-crystal data and, typically in the form of Rietveld refinement, also with powder diffraction data. However, it has been used much less frequently for electron diffraction data. Only in the last decade have electron diffraction tomography (EDT) methods made it possible to reliably determine crystal structure models from electron diffraction data (Kolb *et al.*, 2007, 2008; Wan *et al.*, 2013). However, in the subsequent least-squares refinement, the dynamical diffraction effects, unavoidable in electron diffraction, have been mostly neglected and the data were treated as being kinematical. Despite attempts to limit the departure of the electron diffraction data from the kinematical limit – either by integrating the diffracted intensities using precession electron diffraction (PED; Vincent & Midgley, 1994; Mugnaioli *et al.*, 2009), or by fine-slicing the diffraction spots as in the rotation electron diffraction (RED) method (Zhang *et al.*, 2010), the refinements using this approximation yield high figures of merit and questionable accuracy of the refined structure parameters (Kolb *et al.*, 2011).

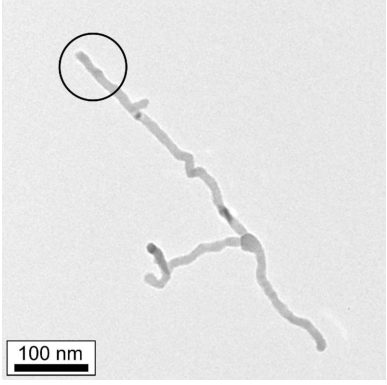

Table 1
Basic crystallographic information and experimental details of the studied samples.

The lattice parameters are those from the reference structures. For mayenite, the number of independent atoms does not include two partially occupied atomic positions.

Sample	Ni_2Si	$PrVO_3$	Kaolinite	Orthopyroxene	Mayenite
Space group	*Pnma*	*Pnma*	*C*1	*Pbca*	$I\bar{4}3d$
a (Å)	5.000	5.561	5.154	18.302	11.979
b (Å)	3.726	7.777	8.942	8.882	11.979
c (Å)	7.053	5.486	7.401	5.208	11.979
α (°)	90	90	91.69	90	90
β (°)	90	90	104.61	90	90
γ (°)	90	90	89.82	90	90
V_{uc} (Å^3)	131.4	237.2	329.9	846.6	1718.9
No. of independent atoms	3	4	13	12	5
TEM acceleration voltage (keV)	120	120	120	200	120
Resolution ($\sin\theta/\lambda$, Å^{-1})	0.7	0.7	0.7	1.0	0.7
No of recorded frames	74	111	101	96; 91	105
Tilt step (°)	1.0	1.0	1.0	1.0	1.0
Precession angle φ (°)	1.5	2.0	1.0	1.2; 2.0	2.0
Data completeness (%)	57.9	97.9	62.1	71, 5; 70.9	99.6
Size of the (illuminated part of the) crystal (nm^2)	15 × 95	70 × 70	380 × 214	200 × 200	600 × 600

Attempts to use the full dynamical diffraction theory in the least-squares refinement (dynamical refinement for brevity) have already been made (Jansen *et al.*, 1998; Dudka *et al.*, 2008; Oleynikov, 2011). In a recent publication (Palatinus *et al.*, 2013, denoted Paper I hereafter), we have first shown that it is advantageous to perform the dynamical refinement against data collected with precession electron diffraction. However, these refinements have so far always been performed on oriented diffraction patterns, while for a robust and complete structure refinement it is necessary to refine the structure against a three-dimensional data set, and ideally to maintain a high data-to-parameter ratio.

With the advent of precession electron diffraction tomography (PEDT), where both PED and EDT techniques are combined, it has become natural to apply the full dynamical theory to the refinement of PEDT data. Recently developed and implemented in *JANA*2006 (Petříček *et al.*, 2014), the basics of the method for dynamical least-squares refinement against PEDT data have been described in a previous publication (Palatinus *et al.*, 2015, denoted Paper II hereafter). The method uses the Bloch-wave formalism to calculate the diffracted intensities in each frame, oriented or non-oriented, as well as the derivatives of the intensities with respect to the structure parameters, and these quantities are used in the standard full-matrix least-squares refinement. In the present contribution we demonstrate the application of the method to five materials. For each material a good-quality reference structure is available, either from the literature or from our own experiment. This allows us to demonstrate the accuracy, advantages and also limitations of the method.

2. Data collection and data processing

The data sets presented in this work were collected on three different transmission electron microscopes with a data collection strategy ranging from fully automated to fully manual. Attributes specific to each data collection are described for each example separately. Common features are the following: a suitable crystal or part of a larger crystal giving a good diffraction pattern was found. A selected precession angle was set, and the precession was aligned and switched on. Then the goniometer was tilted to the maximum tilt, a diffraction pattern was taken and saved, the goniometer was tilted by 1° and another diffraction pattern was taken. The position of the crystal was checked every few degrees and, if necessary, the crystal was moved to stay in the beam. The minimum tilt range among the six presented data sets is 74°, the maximum is 111°.

The data were processed with the program *PETS* (Palatinus, 2011). The procedure differs very little from the standard processing of X-ray diffraction data. The frames were first searched for diffraction maxima. Then the positions were recalculated to the three-dimensional coordinates in reciprocal space, and a difference vector space was calculated from the obtained vectors, similarly to the procedure described in Kolb *et al.* (2008). The graphical interface for indexing available in *JANA*2006 was then used to find the lattice parameters and the orientation matrix of the crystal. Using this matrix, reflection intensities were integrated in PETS. Two integrations were performed. The first type is useful for the structure solution and kinematical refinement. In this integration, intensities belonging to the same reflection on adjacent frames are integrated together, and the resulting list of intensities contains one entry per each *hkl* triplet. The second type of integration, used later for the dynamical refinement, integrates the intensities on a per-frame basis. All reflections with excitation errors smaller than a user-defined limit (0.04 Å^{-1} in the current case) are integrated on every frame. The output is an *hkl*-intensity list with, possibly, several entries for one *hkl* triplet, each integrated on a different frame. Frame number is assigned to each entry in the list.

3. Sample description

There are five samples included in this study – kaolinite, orthopyroxene, mayenite, Ni_2Si and $PrVO_3$. The basic crystallographic and experimental details of all samples are summarized in Table 1. The crystal structures of all samples are shown in Fig. 1.

3.1. Ni_2Si

Ni_2Si crystallizes in the space group *Pnma* with three independent atoms in the unit cell. The PEDT experiment was

Table 2
Experimental details of the single-crystal X-ray data collection on Ni_2Si.

Space group	*Pnma*
a (Å)	4.9996 (7)
b (Å)	3.7261 (4)
c (Å)	7.0532 (9)
V_{uc} (Å^3)	131.39 (3)
λ (Å)	0.071069
Resolution (d_{min}, Å)	0.714
Density (g cm^{-3})	7.35
μ (mm^{-1})	28.768
Crystal dimensions (mm^3)	0.208 × 0.178 × 0.103
Instrument	Agilent Xcalibur Atlas Gemini ultra
Absorption correction	Analytical (*CrysAlisPro*; Agilent, 2014)
R_1(obs), *wR*(all), GOF(all)	0.0194, 0.0257, 1.31
Θ_{max} (°)	29.104
Completeness (%)	98.02
Max., min. Fourier density (e Å^{-3})	0.54, −0.62

performed on a thin nanowire synthesized by the chemical vapor deposition method by the deposition of ethylsilane on nickel substrate at 823 K. The diameter of the wire was approximately 15 nm. The experiment was performed on a Philips CM120 TEM (120 K, LaB_6) with a Nanomegas Digistar precesssion device and a side-mounted Olympus Veleta CCD camera with 14-bit dynamic range.

The structure of Ni_2Si was first published by Toman (1952), who used a Weissenberg camera. Later a model obtained from powder X-ray diffraction data was published by Landrum *et al.* (1998). To have a reference structure of higher accuracy for comparison, we synthesized bulk Ni_2Si material and carried out a single-crystal X-ray structure analysis. The bulk Ni_2Si alloy was prepared from pure elements by arc melting under an argon atmosphere. Samples were homogenized by four times repeated remelting. The samples have a single-phase microstructure with elongated grains caused by rapid cooling on copper plate. The composition was checked *via* energy dispersive spectroscopy and found to be the expected one. Details of the single-crystal data collection and refinement can be found in Table 2. The figures of merit and flatness of the difference Fourier map indicate a good quality refinement and therefore, most likely, also a reliable reference structure model.

3.2. $PrVO_3$

Transition metal oxides (TMO) with a perovskite structure display rich functional properties where atomic displacements, promoted by structural changes associated with orbital occupancy and electron transfer between neighboring sites, play an important role. In these systems, the accurate knowledge of the crystal structure is a key point to understand these coupling mechanisms. To this point the prototypical RVO_3 perovskites (*R* = rare-earth or yttrium) are an interesting class of materials for exploring and exploiting orbital physics in correlated oxides (Miyasaka *et al.*, 2003).

$PrVO_3$ was selected as a representative member of the RVO_3 series. It crystallizes in the space group *Pnma* with four independent atomic positions in the unit cell (1 Pr, 1 V and 2 O) with the V position fixed by symmetry. The sample was prepared by solid-state reaction using a two steps procedure. Stoichiometric amounts of Pr_6O_{11} and V_2O_5 were mixed, pressed into pellets, and heated in air at 1373 K for 48 h in order to first form $PrVO_4$. After an intermediate grinding, the powder was pressed into pellets and heated in Ar:H_2 gas flow at 1223 K for 24 h to form $PrVO_3$. For TEM analyses, a small quantity of the powder was crushed in an agate mortar to obtain small fragments that were put in a suspension in

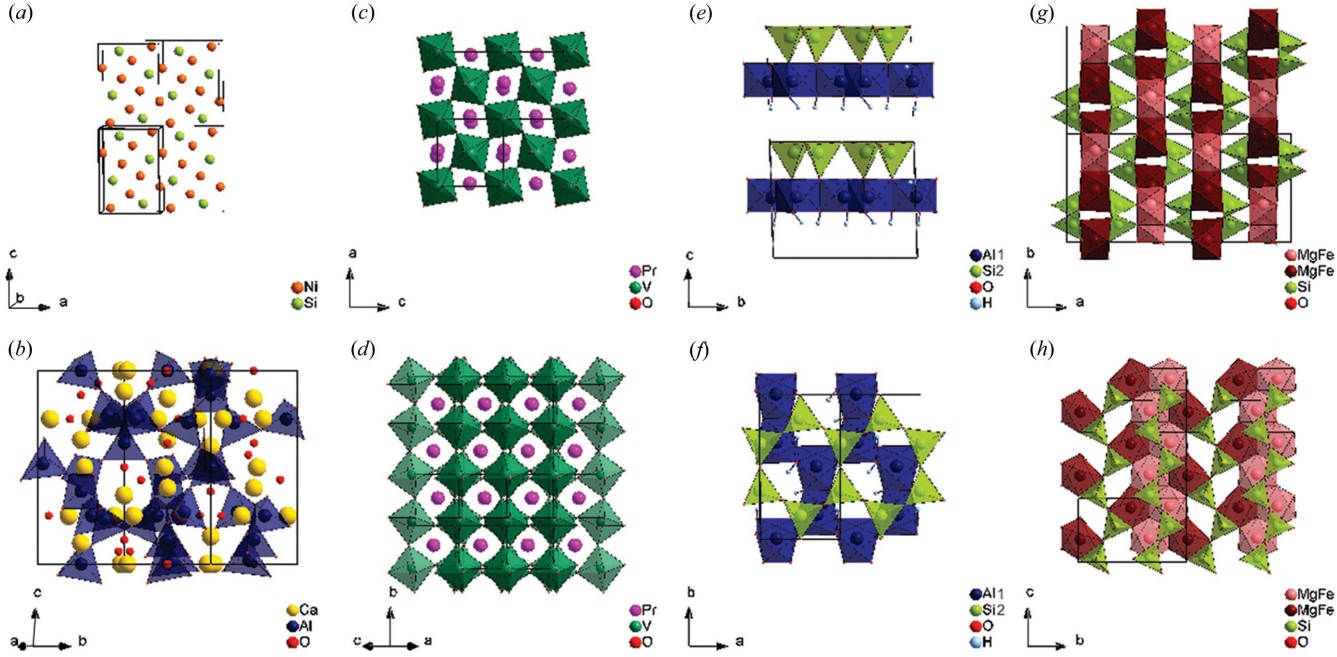

Figure 1
Overview of the crystal structures of the investigated samples: Ni_2Si (*a*), mayenite (*b*), $PrVO_3$ (*c*, *d*), kaolinite (*e*, *f*), orthopyroxene (*g*, *h*).

alcohol. A drop of the suspension was then deposited and dried on a copper grid with a thin film of amorphous carbon.

The data collection was performed on the same Philips CM120 TEM used for the Ni_2Si example.

The reference structure was obtained from a refinement against neutron powder diffraction data (Martínez-Lope *et al.*, 2008).

3.3. Kaolinite

Kaolinite is a sheet silicate mineral with ideal composition $Al_2Si_2O_5(OH)_4$. The structure of kaolinite is noncentrosymmetric, space group $C1$ (a non-standard setting of the space group $P1$), and it contains 13 symmetry-independent non-H atoms in the unit cell. A natural kaolinite sample from Gold Field (Tanzania) was used for the data collection. Details about the sample are given in Smrčok *et al.* (2010). The data set was collected on the same Philips CM120 microscope as was used for the Ni_2Si example (§3.1). The TEM sample was prepared by dispersing the powdered sample in ethyl alcohol. After sonication a drop of the dispersion was put on a holey carbon-coated copper grid. The reference structure was obtained by single-crystal synchrotron X-ray diffraction (Neder, 1999).

3.4. Orthopyroxene

Orthopyroxene is an Fe–Mg-bearing inosilicate mineral with the general formula $(Mg_xFe_{1-x})_2Si_2O_6$ from the group of pyroxenes with a structure formed by single chains of corner-sharing SiO_4 tetrahedra. Every two chains are linked together by a ribbon of $M1O_6$ octahedra ($M1 = Fe^{2+}, Mg^{2+}$). These units are linked together by distorted $M2O_6$ octahedra ($M2 = Fe^{2+}$, Mg^{2+}). Pyroxenes are important rock-forming minerals, which usually contain variable proportions of Mg^{2+} and Fe^{2+} distributed among $M1$ and $M2$ octahedra. The distribution of cations among these sites can be used as a geothermometer (Stimpfl *et al.*, 1999). As the mineral often forms very small grains, electron diffraction is an attractive method for their analysis, provided it allows the determination of the occupancies with sufficient accuracy. The possibility of using PED data for this purpose was demonstrated in previous works using two-dimensional oriented electron diffraction patterns (Jacob *et al.*, 2013; Palatinus *et al.*, 2013). In this work we use one of the previously studied samples.

The sample was obtained from a single crystal of natural orthopyroxene (a few hundred microns in size) from granulite rocks of the Wilson Terrane, North Victoria Land, Antarctica (Tarantino *et al.*, 2002). The average crystal composition as obtained by electron microprobe corresponds to x close to 0.7. In order to obtain a homogeneous and disordered structure regarding mixed site occupancies, the monocrystal has been heated for 48 h at 1273 K and rapidly water-quenched. The crystal was then analysed by single-crystal X-ray diffraction to obtain a reference structure (Jacob *et al.*, 2013).

A thin slab of the sample with thickness less than 100 nm was cut from the crystal perpendicular to the [001] direction using a focused ion beam. TEM observations were performed on an FEI Tecnai G2 20 TEM (200 kV, FEG) equipped with a NanoMEGAS Digistar precession device and an ORIUS 832 Gatan CCD camera with 14-bits dynamic range.

3.5. Mayenite

Mayenite is a mineral name for a cubic aluminate with nominal composition $Ca_{12}Al_{14}O_{33}$ also known in cement chemistry as $C_{12}A_7$. Mayenite has a zeolite-like structure with a framework formed by a three-dimensional network of AlO_4 tetrahedra and CaO_6 distorted trigonal prisms. 64 out of 66 O atoms in the unit cell belong to the Al–Ca–O framework, which forms cages 5–6 Å in diameter. The remaining two O atoms, known as 'free' or 'excess' O atoms, are statistically distributed inside 1/6 of these cages and they are located near the center of the cage being therefore quite loosely coordinated with the framework cations. The consequent mobility of these oxygen allows an easy substitution with other anions producing materials with very interesting properties (Hayashi *et al.*, 2004; Li *et al.*, 2005; Kim *et al.*, 2007).

Mayenite was synthesized by melting a stoichiometric mixture of CaO and Al_2O_3 at 1723 K. The melt was cooled down at 50 K h^{-1} to 1573 K and then quenched. The TEM sample was prepared by grinding the quenched mixture in an agate mortar and dispersing the powder in isopropyl alcohol. After sonication a drop of the dispersion was put on a holey carbon-coated copper grid. PEDT data were collected on a Zeiss Libra 120 TEM (120 kV, LaB_6 cathode) equipped with an in-column omega filter for energy-filtered imaging, a Nanomegas Digistar P1000 for precession electron diffraction and a bottom mounted TRS 2kx2k 14-bit CCD camera. Two data sets were collected on the same crystal, with and without energy filtering. The energy-filtered data were collected with a 20 eV slit centered on the zero-loss peak. Except for the use of the energy filter, the experimental setting was identical for both data collections.

Several works discussed the structure of mayenite. We have found only one that determined the structure from a single-crystal diffraction experiment and was performed at ambient conditions (Sakakura *et al.*, 2011). However, this structure determination is very detailed – the structure model contains five major atomic positions and eight additional positions with partial occupancy. It would be complicated to compare this structure model with the PEDT refinement. Therefore, we have selected the structure model published by Boysen *et al.* (2007) using high-quality neutron powder diffraction data as a reference structure. This model contains only two partially occupied atomic positions. Both these positions have low occupancy – one Ca atom with occupancy 0.125 and one O atom with occupancy 0.251. In the test refinements we decided to ignore these two positions. The detectability of these partially occupied positions from the PEDT data will be discussed in §5.5.

4. Strategy of the test refinements

It is one of the aims of this work to find the best parameters and guidelines for the use of the dynamical refinement method. Therefore, we performed an extensive set of test refinements on each sample data set. This section describes the procedure, which has been applied to each data set.

The dynamical refinement has a range of specific parameters, as discussed in detail in Paper II. Here we give only a brief overview. The parameters can be divided into two classes: the data selection parameters and the parameters influencing the calculation of model intensities. The data selection parameters are the most specific category which does not have a direct counterpart in X-ray diffraction analysis. These parameters are used to select a set of reflections included in the refinement for each frame. Two parameters are available: $S_g^{\max}$, the maximum excitation error of an included reflection, and $R_{S_g}^{\max}$, the maximal allowed ratio between S_g and the maximum amplitude of the precession motion. The former parameter defines a band of constant thickness around the Ewald sphere, and is independent of the precession angle. The larger $S_g^{\max}$, the more reflections are included with increasing distance from the Ewald sphere, and hence with, generally, lower intensity. The parameter $R_{S_g}^{\max}$ is specific to precession data. It also imposes a limit on the distance of a reflection from the Ewald sphere, but this time this distance is compared with the amplitude of the precessing motion, and only reflections closer to the Ewald sphere than a certain fraction of the precession amplitude are included. This parameter, as will be seen later, is of crucial importance for the refinement. A more detailed definition of $R_{S_g}^{\max}$ can be found in Paper II.

The parameters influencing the calculation of model intensities specify the list of beams entering the structure matrix, which is then used for the calculation of the dynamical intensities. The two parameters are $g_{\max}$ – the maximum length of the diffraction vector, and $S_g^{\max}$ – the maximum excitation error of the reflections used to build the structure matrix. To differentiate the two limits on excitation errors, we denote the limit for the structure matrix as $S_g^{\max}$(matrix), while the data selection parameter specifying the experimental data to be included in the refinement is $S_g^{\max}$(refine). The third parameter, N_{steps}, is specific to the precession electron diffraction and specifies the number of evaluations of diffracted intensities along the precession circuit.

For each sample the following refinement procedure was applied:

(i) Using the kinematical intensity integration, the structure was solved using the program *SUPERFLIP* (Palatinus & Chapuis, 2007) interfaced from *JANA*2006. The structure model was corrected, if necessary, by removing spurious atoms and changing the chemical types of atoms.

(ii) This model was refined using a kinematical approximation without any constraints. The result of this refinement is denoted as a kinematical model.

(iii) The data obtained by the dynamical intensity integration were combined with the kinematical model to yield a starting point for dynamical refinement. If the displacement parameters of some atom refined to an unrealistic value (too large or negative), it was set to a more reasonable value.

(iv) An initial estimation of the sample thickness was performed for each frame by calculating the weighted R value on amplitudes (wR_1) for a given frame as a function of the thickness. The thickness giving the best wR_1 was taken as the best estimate of the thickness for the frame. An initial estimate of the overall sample thickness was then obtained as an average over all frames. Each data set in this work stems from one particle and therefore a constant thickness was assumed for all frames, corrected only for the change of thickness along the incident beam caused by the sample tilt.

(v) A least-squares structure refinement was performed. Refined parameters included atomic coordinates, isotropic displacement parameters and scale factors of individual frames. The refinement (as well as all other refinements) was conducted until convergence. The refinement parameters were set to the default values which were established in previous preliminary tests of the method. These parameters were $S_g^{\max}(\text{refine}) = 0.025$, $R_{S_g}^{\max} = 0.75$, $S_g^{\max}(\text{matrix}) = 0.01$, $g_{\max}(\text{matrix}) = 2.0$ and $N_{\text{steps}} = 128$. This refinement was considered as the reference dynamical refinement, a starting point for further systematic tests.

(vi) Using the reference dynamical refinement as the starting model, a series of test refinements was performed with all but one parameter kept fixed, and the remaining parameter varied to find its optimal value. The optimized parameters involved $S_g^{\max}$(refine), $R_{S_g}^{\max}$, $S_g^{\max}$(matrix), $g_{\max}$(matrix) and N_{steps}. For every setting, the structure was refined to convergence. Then an orientation optimization was performed. This optimization was performed on each frame by searching for the minimum of wR_1 as a function of the tilt of the normal to the recorded plane (*i.e.* zone axis, as it would be called in the case of oriented patterns). A downhill simplex algorithm was used for the optimization. The procedure was described in detail in Paper I. The optimized tilts were checked and possible outliers removed from the list of frames, as discussed in §5. After the orientation optimization another structure refinement was performed.

(vii) Possible additional refinements were performed, if considered useful for a given data set.

To evaluate the model stemming from different refinements, the following values were considered:

(i) Refinement R values R_1(obs) and wR_1(all).

(ii) Comparison with the reference structure. For each structure a reference high-quality structure model obtained by X-ray or neutron diffraction was available either from the literature or from our own experiment. Each refined structure model was compared with the reference structure by means of the average and maximum distance between an atom and the corresponding atom in the reference structure. These two quantities will be denoted as the average distance from reference atoms (ADRA) and the maximum distance from reference atoms (MDRA). Atoms with positions completely fixed by symmetry were not included in the calculation of ADRA.

Using the default refinement parameters, another refinement was performed using the two-beam model, as suggested by Sinkler *et al.* (2007) and used already in Paper I. In this model the intensity of each beam is calculated using the approximation that this beam and the primary beam are the only two beams excited in a given orientation. This model has the important property that it uses the same data and the same number of parameters as the full dynamical refinement, and thus allows a more direct comparison with the dynamical refinement than the kinematical refinement, where the number of parameters and data points is very different.

Finally, for every model the structure model resulting from kinematical refinement was also evaluated for comparison.

5. Results of the test refinements

The large number of test refinements was performed with the aim of understanding the role of different parameters on the accuracy of the refinement and to obtain the overall idea about the achievable accuracy. The complete tables are available as supporting information. Here we summarize the general observations and trends, and comment on the optimal parameter settings. In the subsequent subsections we will comment on the particularities of each studied example.

Table 3
Summary of refinement results on all tested data sets with different calculation parameters and models for calculation of I_{calc} (OO represents orientation optimization).

Data set/refinement	R_1(obs)	wR_1(all)	N_{obs}	N_{all}	N_{par}	ADRA (Å)	MDRA (Å)
Ni_2Si							
Kinematical	11.07	11.53	88	118	10	0.0206	0.0240
Two-beam	8.24	10.94	718	1628	72	0.0126	0.0188
Dynamical without OO	9.74	12.65	868	1963	84	0.0087	0.0129
Dynamical	7.28	10.20	753	1713	75	0.0076	0.0110
Dynamical with ADP	6.87	10.34	805	1864	86	0.0058	0.0089
Dynamical cylinder	7.25	10.34	721	1660	73	0.0073	0.0106
$PrVO_3$							
Kinematical	24.04	26.43	197	369	12	0.1549	0.2395
Two-beam	13.26	17.11	1267	4113	112	0.0247	0.0397
Dynamical without OO	11.81	14.55	1419	4684	123	0.0200	0.0362
Dynamical	9.11	12.21	1403	4599	123	0.0174	0.0298
Dynamical with ADP	9.08	12.15	1403	4599	139	0.0156	0.0282
Kaolinite							
Kinematical	19.15	20.17	941	1062	53	0.0946	0.2660
Two-beam	9.48	11.04	1667	2184	154	0.0648	0.1544
Dynamical without OO	7.88	8.62	1677	2205	154	0.0223	0.0498
Dynamical	5.77	6.08	1650	2177	153	0.0216	0.0504
Dynamical with ADP	5.45	5.71	1650	2177	218	0.0232	0.0531
Dynamical inverted	8.19	8.84	1649	2174	153	0.0316	0.0763
Opx $\varphi = 1.2^\circ$							
Kinematical	24.98	27.61	821	2558	43	0.0492	0.0814
Two-beam	16.10	18.52	2170	17666	132	0.0527	0.0946
Dynamical without OO	8.42	10.27	2235	18038	133	0.0127	0.0236
Dynamical	6.01	7.48	2209	17991	133	0.0104	0.0193
Dynamical with ADP	5.85	7.27	2229	18079	183	0.0104	0.0236
Opx $\varphi = 2.0^\circ$							
Kinematical	24.18	26.09	700	2586	43	0.0493	0.0782
Two-beam	16.95	19.23	2904	29224	133	0.0626	0.1104
Dynamical without OO	9.30	11.44	2876	29765	133	0.0164	0.0575
Dynamical	7.06	8.91	2774	28446	131	0.0142	0.0263
Dynamical with ADP	6.69	8.01	2812	28822	182	0.0158	0.0251
Mayenite							
Kinematical	17.56	20.90	268	420	12	0.0270	0.0392
Two-beam	11.30	16.74	2027	10677	113	0.0200	0.0390
Dynamical without OO	10.44	14.63	2115	11149	117	0.0155	0.0402
Dynamical	8.63	12.69	2125	11062	116	0.0121	0.0334
Dynamical with ADP	8.25	12.39	2125	11062	127	0.0136	0.0319
Dynamical inverted	12.53	17.84	2127	11173	117	0.0238	0.0462
Dynamical filtered	8.68	14.27	1662	10622	112	0.0220	0.0408

The most important refinement results are summarized in Table 3. The principal general observation is that the result of the dynamical refinement is always better than the kinematical refinement, both in terms of the *R* values and, more importantly, in terms of ADRA. The ADRA of the dynamical refinement is on average more than four times smaller than for kinematical refinement, the improvement ranging from a factor 2.2 (mayenite) to almost 9 ($PrVO_3$). The largest ADRA is 0.022 Å and the largest MDRA is 0.050 Å (both in kaolinite). In contrast, ADRA for kinematical refinement may be surprisingly low in some cases (0.021 Å for Ni_2Si, 0.027 Å for mayenite), but may reach very high values (0.095 Å for kaolinite, 0.155 for $PrVO_3$).

The results of the two-beam refinement are almost always better than the kinematical results, but they do not approach the quality of the full dynamical refinement. This is an important observation. It demonstrates that the improvement of the structure model is not caused by the larger number of refined parameters due to the separate scale factor on every frame. The number of refined parameters, data selection parameters and separate scales for each frame are common to the two-beam and dynamical refinements. The accuracy of the dynamical refinement thus indeed stems from the employment of the full dynamical diffraction theory.

Another interesting observation is that the accuracy of the structure model is relatively insensitive to the choice of the computation and data selection parameters, as long as they remain within reasonable limits. While the *R* values change quite a lot with changing data selection parameters, the ADRA remains relatively stable. The influence of individual parameters can be summarized as follows:

(i) $R_{S_g}^{max}$: The setting of this parameter has the largest influence of all the parameters on the accuracy of the refined model. Values larger than 0.8 lead almost always (with one exception – Ni_2Si) to a dramatic increase of the *R* values and

ADRA. On the other hand, setting $R_{S_g}^{\max}$ to small values (and thus limiting the number of reflections in the refinement to those very close to the Bragg condition) does not degrade the quality of the structure model, and sometimes very good results are obtained with $R_{S_g}^{\max}$ as low as 0.15. However, with low $R_{S_g}^{\max}$ the data-to-parameter ratio decreases and at a certain moment the low number of reflections will negatively affect the accuracy of the refinement. We recommend that $R_{S_g}^{\max}$ is set to 0.4, unless the number of reflections with significant intensity is lower than 10× the number of refined parameters. In such a case the value of $R_{S_g}^{\max}$ should be increased to exceed that limit.

(ii) $S_g^{\max}$(refine): This data selection parameter correlates strongly with $R_{S_g}^{\max}$. The test refinements show that the best results are obtained if it is set to a large number, effectively infinity, and the data selection can be based entirely on $R_{S_g}^{\max}$. In practice, setting $S_g^{\max}$(refine) to infinity is equivalent to setting it to a value larger than $R_{S_g}^{\max} \cdot g_{\max} \cdot \varphi$. A value of 0.3 Å^{-1} is equivalent to infinity for all practical purposes. Note that this method cannot be used for data without precession, where R_{S_g} is zero for all reflections. For data without precession, $S_g^{\max}$(refine) should be set to a value large enough to include a sufficient number of intensities in the refinement. A value of 0.01 Å^{-1} should be appropriate in most cases.

(iii) $S_g^{\max}$(matrix): This is a computation parameter and the expected behavior would be that with an increasing value the accuracy improves (ADRA decreases). Surprisingly, the tests show that with increasing $S_g^{\max}$(matrix) above *ca* 0.01 Å^{-1} the ADRA tends to rise in many cases. We do not have any explanation for this observation, we just note that a similar behavior was already observed in Paper I. We conclude that the best value of $S_g^{\max}$(matrix) appears to be 0.01 Å^{-1}.

(iv) N_{steps}: The refinement is remarkably insensitive to this parameter. Values as low as 32 still provide acceptable results. However, it is recommended that a larger value be used, *e.g.* 96, during the refinement. An even larger number like 128 should be used for the last few refinement cycles to obtain a more accurate result at the cost of longer computing time. Rarely, especially for thicker samples containing heavier elements, an even larger number may be needed.

(v) $g_{\max}$: Also this parameter influences the refinement only weakly. $g_{\max}$ must always be larger than the maximum experimental value, but need not be much larger than that. For a standard data set with resolution $g_{\max}^{\text{exp}}$ = 1.4 Å^{-1} a value of 1.5 Å^{-1} is acceptable. For the final calculation $g_{\max}^{\text{exp}}$ = 2.0 Å^{-1} may be recommended as a safe value. Higher values do not improve the accuracy and only increase the calculation time.

The results in Table 3 were obtained with these recommended parameters, *i.e.* $S_g^{\max}$(refine) = ∞, $S_g^{\max}$(matrix) = 0.01 Å^{-1}, $g_{\max}$ = 2.0 Å^{-1}, N_{steps} = 128 and $R_{S_g}^{\max}$ = 0.4 whenever the number of significant reflections was larger than 10× the number of parameters (mayenite, both orthopyroxene data sets), and higher otherwise – 0.65 for kaolinite, 0.75 for Ni_2Si and 0.5 for $PrVO_3$.

As mentioned earlier, the refinement also includes the scale factors of individual frames. Refining individual scale factors is necessary, because there are many factors that influence the overall scale of each frame and that are essentially unpredictable, like the illuminated area of the crystal (which may change quite a lot from frame to frame, if only part of the crystal is illuminated by the beam), varying thickness and thus absorption, possible variation of the primary beam intensity or slowly growing contamination of the crystal. As a result of all these effects the scale may vary quite significantly from frame to frame. Moreover, as intensities of symmetry-related reflections are not expected to be equal, frame scaling prior to data reduction, which is often used in X-ray diffraction, cannot be used. The scale typically varies by less than 10% from one frame to the next, but an overall trend of the scale factor can be observed in most samples, corresponding most likely to the changes in the illuminated area of the crystal.

An important part of the refinement process is the optimization of the orientations of individual frames. As described already in Paper I and Paper II, this optimization must be performed separately from the least-squares refinement, because the minimized function is not smooth with respect to the orientation parameters. There are several effects that may cause the orientation of a frame as calculated from the orientation matrix to be inaccurate. It may be the limited accuracy of the microscope goniometer, the inaccuracy of the orientation matrix itself or small unpredictable movements of the crystal under the electron beam. Our tests show that the optimization of frame orientations is indeed beneficial. In all cases it leads to better R values and, more importantly, to lower ADRA values. The deviation of the orientation from the original orientation as calculated from the orientation matrix is expected to be small, only a fraction of a degree. In practice, this is mostly fulfilled and the corrections to the tilt angle are typically around 0.1 or 0.2°. Occasionally, however, the orientation parameters may diverge to much larger values, sometimes up to 1°. This happens especially for structures with very small unit cells and consequently a low average number of reflections per frame, and may be attributed to the instability of the optimization of certain frames due to a very small number of reflections or due to the presence of a very strong reflection that dominates the optimization process. To avoid using clearly aberrant results, we decided to eliminate from the refinement all frames for which optimization of orientation resulted in a tilt away from the original position larger than 0.5°. In most data sets this affected at most one or two frames, except for Ni_2Si, where eight out of 74 frames had to be removed. This data set has a low number of observed reflections due to the weak signal from a thin nanowire. Moreover, the unit cell is the smallest of all tested structures, and the number of reflections per frame is thus very small. Despite these unfavorable circumstances and removal of a number of frames the orientation optimization improves the refinement result visibly. If the number of frames eliminated by this procedure should be too large, it may mean that the data are not suitable for the optimization of orientation, and it may be advisable to refrain from the orientation optimization entirely.

In all cases we also tried to refine anisotropic displacement parameters (ADPs). In many cases the result is good and

ADPs are positive definite. However, in kaolinite and also in orthopyroxene the ADPs of some atoms refine to non-positive definite tensors. In both these cases the largest ADPs are U^{33}, and the strong anisotropy of the displacement parameters may be attributed to the missing wedge of data.

In the following sections we focus on the specifics of each sample. For each sample we also give approximate computing time per one refinement cycle. Note that typically about ten or fewer cycles are necessary to reach convergence. All reported calculation times were obtained on a standard desktop PC equipped with a six-core Intel Core i7-4930K processor.

5.1. Ni_2Si

The complete set of test refinements is summarized in the supporting information, Tables S1 and S2. The data on the Ni_2Si sample were collected on a single very thin nanowire with diameter ~ 15 nm (Fig. 2). The thin sample is probably also the reason why even the kinematical refinement on this data set results in a surprisingly accurate structure model with ADRA only 0.0204 Å and $R1 = 0.1107$. Nevertheless, the dynamical refinement still improved both the $R1$ value and ADRA significantly.

Most samples presented in this work could be, to a good approximation, treated as flat plates, and this model was also used for them. The refinement included the correction for changing thickness due to the tilting of the plate during the data collection. For the test calculations on Ni_2Si, a plate model was also used, despite the fact that the crystal had the form of a nanowire with approximately cylindrical cross section. We have also performed the refinement assuming a cylindrical shape of the sample, using the simplified model described in Paper II. The result of this refinement is also included in Table 3. The refinement results are only very slightly better than the results with the plate model. This is most likely caused by the small thickness of the sample, but it also demonstrates the insensitivity of the method to the thickness variations in the sample and supports the claim that deviations of the crystal shape from the idealized shape are not detrimental to the accuracy of the refined structure model.

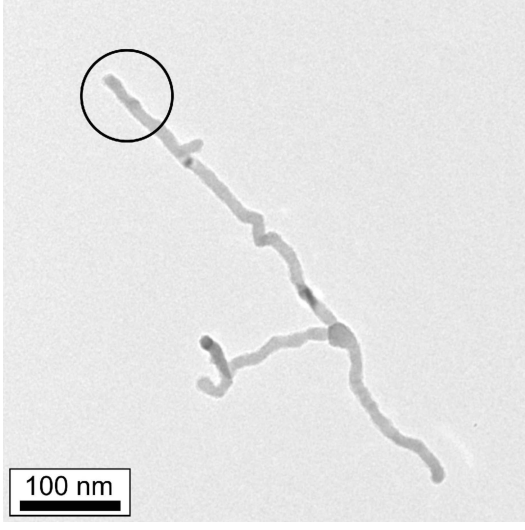

Figure 2
Image of the Ni_2Si nanowire used for the data collection. The diameter of the wire is approximately 15 nm.

In Ni_2Si the refinement of anisotropic displacement parameters leads to the largest relative improvement of the accuracy of all data sets. ADRA decreased from 0.0076 to 0.0058 Å and MDRA from 0.0110 to 0.0089 Å. This makes the results on Ni_2Si the most accurate – in terms of the match with the reference structure – of all the tested samples. It should be acknowledged, however, that this is also the sample with the smallest number of independent atoms in the unit cell – only three. Moreover, the y coordinates of all the atoms are fixed by symmetry. Hence, assuming a homogeneous and random distribution of errors among all coordinates, the ADRA is expected to be by a factor of $\sqrt{3}/\sqrt{2} = 1.22$ smaller than for a structure with all atoms in general positions.

One cycle of the least-squares refinement with the recommended settings took approximately 54 s.

5.2. $PrVO_3$

The results of the test refinements are shown in Tables S3 and S4. $PrVO_3$ shows the largest improvement when moving from kinematical to dynamical refinement – ADRA decreases from 0.1549 to 0.0174, MDRA from 0.2395 to 0.0298, *i.e.* by a factor of 9 and 8, respectively. The accuracy obtained with the dynamical refinement allows a quantitative analysis of the octahedral tilt observed in this distorted perovskite structure.

The refinement of the anisotropic displacement parameters leads to acceptable values of the displacement parameters and to a small improvement of ADRA and MDRA parameters. Despite the small unit-cell volume the orientation optimization was relatively stable and only one frame had to be excluded from the refinement due to the tilt larger than 0.5°.

One cycle of the least-squares refinement with the recommended settings took approximately 112 s.

5.3. Kaolinite

The complete set of test refinements is summarized in Tables S5 and S6. The kaolinite example is notable in three aspects: it is a low-symmetry structure (space group $C1$), it is non-centrosymmetric, and it contains H atoms.

The refinement results are satisfactory despite the relatively low completeness of the data – ADRA obtained with the recommended parameters is 0.0216 Å. The only major problem appears to be the refinement of anisotropic displacement parameters. While isotropic parameters refined all to reasonable positive values, the anisotropic refinement led to non-positive definite tensors of displacement parameters for six atoms, with the largest eigenvalue along the $\mathbf{c}^*$ direction and a negative eigenvalue close to the *ab* plane. The $\mathbf{c}^*$ is the central axis of the missing wedge in the data set. The incompleteness of the data along $\mathbf{c}^*$ may be one reason for this problem. The other may be that kaolinite is a layered material with frequent occurrence of stacking faults. Although the sample under investigation is very well ordered, it may contain

a small number of stacking faults, which may have an effect on the intensities that result in the distorted ADP tensors.

Most interestingly, the refinement allowed for an unambiguous identification of the correct absolute structure. Inverting the structure and performing the refinement with default parameters (including the optimization of orientations) leads to $R1$(obs) = 0.0819, a value significantly higher than 0.0577 for the correct structure. Note that this difference does not stem from resonant scattering effects, as in the determination of absolute structure with X-ray diffraction data, but stems directly from the nature of dynamical diffraction, which does not preserve Friedel's law even in the absence of any resonant scattering.

Unfortunately, the refinement was not sensitive enough to allow for the location and refinement of the H atoms. The difference Fourier map contains a maximum at one out of four expected positions of the H atoms (Fig. 3). Placing the H atoms at the positions determined by Neder (1999) does not improve either the R factors, or the ADRA value, and a free refinement of the hydrogen positions leads to large shifts of the H atoms to entirely unrealistic positions.

One cycle of the least-squares refinement with the recommended settings took approximately 144 s.

5.4. Orthopyroxene

The results of the test refinements are summarized in Tables S7 and S8 for the data set with $\varphi = 1.2^\circ$ and in Tables S9 and S10 for $\varphi = 2.0^\circ$. The specialty of the orthopyroxene structure is the mixed occupancy of two cationic sites $M1$ and $M2$, which may be occupied by Fe^{2+} and Mg^{2+}. Two data sets were measured on the same crystal, one with precession angle $\varphi = 1.2^\circ$ and one with $\varphi = 2.0^\circ$. As can be seen in Table 3 and

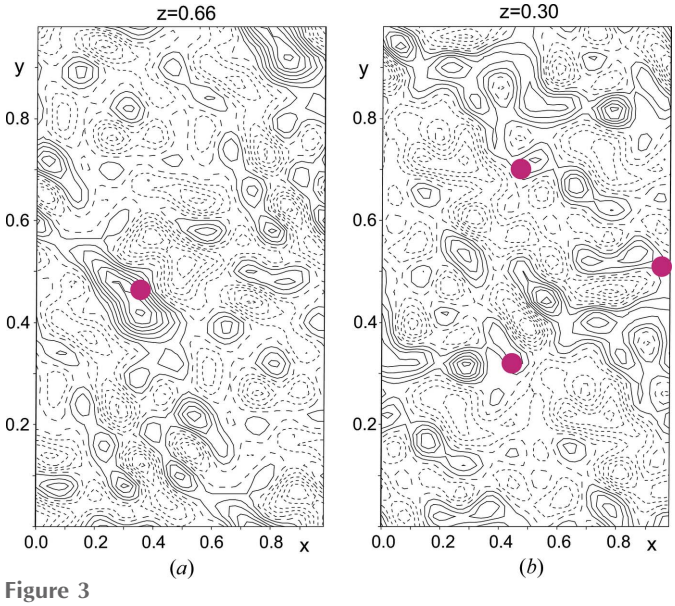

Figure 3
Sections of the difference Fourier map of kaolinite in the two planes containing hydrogen atoms (*cf.* Fig. 1*e*). Expected hydrogen positions are marked with full circles. While one of the expected hydrogen positions is associated with the largest maximum in the difference map (*a*), no significant maxima are visible in the other three positions (*b*).

Table 4
Occupancy of Fe^{2+} atoms at the site $M1$ (Fe1) and at the site $M2$ (Fe2) as obtained from PEDT data and reference X-ray refinement.

Dataset	Occ(Fe1)	Occ(Fe2)
X-ray	0.150 (3)	0.424 (3)
PEDT $\varphi = 1.2^\circ$, dynamical isotropic	0.176 (4)	0.425 (4)
PEDT $\varphi = 1.2^\circ$, dynamical anisotropic	0.165 (4)	0.411 (5)
PEDT $\varphi = 1.2^\circ$, kinematical	0.516 (31)	0.401 (27)
PEDT $\varphi = 2.0^\circ$, dynamical	0.184 (4)	0.428 (4)
PEDT $\varphi = 2.0^\circ$, dynamical anisotropic	0.176 (4)	0.426 (4)
PEDT $\varphi = 2.0^\circ$, kinematical	0.513 (29)	0.389 (24)

Tables S7 and S9, both datasets give good results, however, the former one is noticeably better both in the R values and in the ADRA/MDRA parameters. This is an unexpected result. Based on the results obtained in Paper I we expected the higher precession angle to yield a more accurate structure model. It will require gathering more experience with different structures before firm conclusions can be made about the influence of the precession angle on the result, but from the collection of refinements presented here it appears that, for PEDT data, using a very high precession angle is not crucial and good results can be obtained also with moderate precession angles $\varphi = 1.0^\circ$ or $\varphi = 1.2^\circ$.

It is well known that refinement of the atomic occupancies represents a special challenge in structure refinement. Occupancies tend to correlate with displacement parameters, and especially if one site is occupied by two different atoms and not by a single partially occupied atom, an accurate determination of the occupancy factors is a challenge, particularly if the scattering powers of these two chemical species are not very different. In the orthopyroxene structure there are two such sites: $M1$ and $M2$. The refined occupancies from PEDT and single-crystal X-ray data are summarized in Table 4. It can be seen that the PEDT occupancy of Fe at $M2$ (atom name Fe2) is almost identical with the reference (within 1 e.s.d.), while the occupancy of Fe at $M1$ (atom name Fe1) is somewhat higher than the reference, if isotropic displacement parameters are refined. An anisotropic refinement leads to an improved occupancy of Fe1, which is now only 1.5% and 2.6% different from the reference for $\varphi = 1.2^\circ$ or $\varphi = 2.0^\circ$, respectively. Such an agreement can be considered to be very good, although, strictly speaking, when $\varphi = 2.0^\circ$, the difference is significant at the level of 5.7σ. In contrary, the occupancies refined with kinematical refinement are entirely unreliable for the $M1$ site. Interestingly, the occupancy of the $M2$ site is not so divergent. The reason may be that the occupancies of the two sites depend in a different way on the structure factors of a few low theta reflections, which have a very strong leverage in a full-matrix least-squares refinement (Merli *et al.*, 2002). A strong deviation of a small number of intensities from the kinematical limit, which is frequent in EDT data, may have a strong effect on the refined occupancy of one site, but not so much on the other one.

One cycle of the least-squares refinement with the recommended settings took approximately 2280 s (38 min). It is noteworthy, however, that out of this time almost half (17 min)

was spent on ten frames in the vicinity of the [001] zone. On these frames the number of excited beams is much larger than on other frames, and the computing time is correspondingly longer. For the sake of the computing time it is thus advisable to avoid recording of oriented patterns in the EDT data set.

5.5. Mayenite

The results of the test calculations are shown in Tables S11 and S12. Because the test calculations were numerous and, due to the relatively large unit-cell dimension, also time consuming, they were performed with only even frames included in the refinement. Tables 3 and S12, however, contain refinements performed on the complete set of frames.

Mayenite is known as an ionic conductor. It is also known to have a complicated structure, with partially occupied Ca and O positions. It is therefore difficult to compare various structure models. Nevertheless, the agreement with the reference structure (Boysen *et al.*, 2007) is good, with ADRA = 0.012 Å. This result may be compared with other structure determinations of the same material using different techniques. The mutual fits of different published structure models using only the five major atomic positions are summarized in Table 5. The table shows that the ADRA among five different literature structures ranges from 0.007 to 0.017 Å (one structure, Büssem & Eitel, 1936, was left out as a clear outlier), while the comparison of these structures with PEDT model (column 7 in Table 5) ranges from 0.012 to 0.026 Å. The spread is larger for PEDT data, but not dramatically. It is another indication that the current method provides results with accuracy that approach the accuracy of established methods.

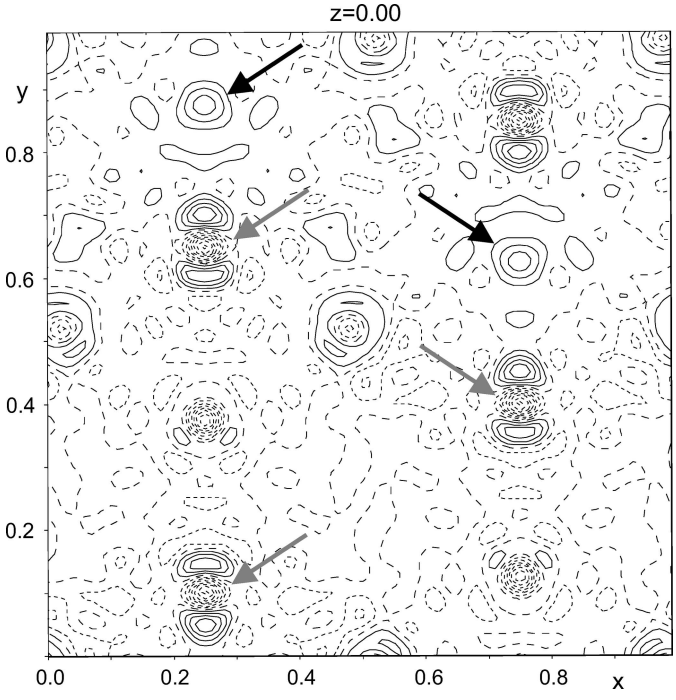

Figure 4
Difference Fourier map of mayenite at the level of Ca and the O3 atom. A clear maximum is observed at the expected positions of the partially occupied O atom (marked by black arrows), and a pair of maxima indicating possible splitting of the position is visible at the positions of the Ca atom (marked by grey arrows).

Table 5
Comparison of ADRA values (in Å) among seven different structure determinations of mayenite.

The numbers in the header row and columns refer to the following references: (1) Büssem & Eitel (1936); (2) Bartl & Scheller (1970); (3) Christensen *et al.* (1987); (4) Stys *et al.* (2006); (5) Boysen *et al.* (2007); (6) Sakakura *et al.* (2011); (7) this work, refinement with recommended parameters.

	1	2	3	4	5	6	7
1	–	0.076	0.061	0.056	0.050	0.063	0.052
2	–	–	0.015	0.007	0.017	0.010	0.019
3	–	–	–	0.011	0.014	0.014	0.019
4	–	–	–	–	0.013	0.008	0.019
5	–	–	–	–	–	0.016	0.012
6	–	–	–	–	–	–	0.026

The difference Fourier map clearly showed a positive peak at the expected position of the partially occupied O atom, and a pair of maxima around the position of the Ca atom (Fig. 4). The maxima around the Ca atom almost disappear if anisotropic displacement parameters are refined. A refinement with a partially occupied O atom in the cage position has been performed. Unfortunately, the isotropic displacement parameter and the occupancy factor of the O atom were strongly correlated and the occupancy could be refined only if the displacement parameter was fixed. When fixing the U_{iso} of the O3 atom to the average value of the other O atoms, the occupancy refines to 0.272 (2), in very good agreement with the value 0.251 (6) obtained by Boysen *et al.* (2007), given the weakness of the feature in question. No trace of the O3 position can be found in the difference Fourier map obtained from the kinematical refinement.

Similarly to kaolinite, also for the mayenite structure the correct absolute structure could be determined. The *R*1 value of the inverted structure rises from 0.0863 to 0.1253.

Apart from the standard data set we measured another data set on the same crystal with the same conditions, but using an energy filter. Such a data set should be, in principle, better than the non-filtered data set, as the contribution of inelastic scattering is removed and the background level is decreased. Interestingly, the refinement on this data set did not lead to an improved structure model. On the contrary, as seen in Table 3, the resulting model is slightly worse in all parameters – *R*1, ADRA and MDRA. The only plausible explanation is that the energy filtering must have introduced some small systematic error in the intensities, which counter-weighted the improvement due to the removal of the inelastic scattering. Further investigations are needed to understand this surprising result, but it is an indication that using filtered data instead of unfiltered is unlikely to bring a major improvement of the accuracy.

One cycle of the least-squares refinement with the recommended settings took approximately 980 s (16 min and 20 s).

6. Conclusions

We have analyzed precession electron diffraction tomography data obtained on five different samples employing the newly developed method of dynamical refinement. We have shown that the new method provides accurate structure models with a typical deviation of atomic positions from the reference structures less than 0.02 Å. Moreover, the refinement allows an observation of fine details like partial occupancies of O atoms, splitting of atomic positions, refinement of mixed occupancies in one site and determination of absolute structure of non-centrosymmetric crystals. The standard deviations on parameters obtained with this method are typically only about three times larger than the corresponding standard deviations obtained from high-quality single-crystal X-ray diffraction studies.

Thorough tests with various settings of the parameters of the method revealed that the refinement is largely insensitive to the exact values of these parameters, as long as they are not set to extreme values. By evaluating the tests, we were able to suggest an optimal set of parameters that appears to work well under common circumstances.

With the present work we provide a firm ground for establishing the power and limitations of the new method of dynamical refinement against PEDT data. We believe that this method with the accuracy demonstrated on the presented examples will change the reputation of structure analysis of nanocrystals and will start an era, when a well refined, accurate and reliable structure model from electron diffraction data will not be a rare achievement reserved to a few specialists, but will become a standard.

Acknowledgements

We thank Ľubomír Smrčok from the Slovak Academy of Science for providing the kaolinite sample, Marco Merlini of Università degli Studi di Milano for the synthesis of the mayenite sample and D. Troadec (IEMN, University Lille 1) for the preparation of orthopyroxene samples by FIB. This work was funded from the grant of the Grant Agency of the Czech Republic No. 13-25747S. LP acknowledges the support of his research through Fellowship J. E. Purkyně awarded by the Academy of Sciences of the Czech Republic. The TEM national facility in Lille (France) is supported by the Conseil Regional du Nord-Pas de Calais, the European Regional Development Fund (ERDF), and the Institut National des Sciences de l'Univers (INSU, CNRS). JK acknowledges the support from the project FUNBIO – CZ.2.16/3.1.00/21568 and MEYS CR LM2011029. PB and GS acknowledge the financial support of the French Agence Nationale de la Recherche (ANR) through the program 'Investissements d'Avenir' (ANR-10-LABX-09-01), LabEx EMC3.

References

Agilent (2014). *CrysAlisPro*. Agilent Technologies, Yarnton, England.
Bartl, H. & Scheller, T. (1970). *Neues Jahr. Mineral.* pp. 547–552.
Boysen, H., Lerch, M., Stys, A. & Senyshyn, A. (2007). *Acta Cryst.* B**63**, 675–682.
Büssem, W. & Eitel, A. (1936). *Z. Kristallogr.* **95**, 175–188.
Christensen, A., Sandström, M., Maartmann-Moe, K., Maberg, O., Scheie, A. & Louër, D. (1987). *Acta Chem. Scand. A*, **41**, 110–112.
Dudka, A. P., Avilov, A. S. & Lepeshov, G. G. (2008). *Crystallogr. Rep.* **53**, 530–536.
Hayashi, K., Matsuishi, S., Hirano, M. & Hosono, H. (2004). *J. Phys. Chem. B*, **108**, 8920–8925.
Jacob, D., Palatinus, L., Cuvillier, P., Leroux, H., Domeneghetti, C. & Cámara, F. (2013). *Am. Mineral.* **98**, 1526–1534.
Jansen, J., Tang, D., Zandbergen, H. W. & Schenk, H. (1998). *Acta Cryst.* A**54**, 91–101.
Kim, S. W., Matsuishi, S., Nomura, T., Kubota, Y., Takata, M., Hayashi, K., Kamiya, T., Hirano, M. & Hosono, H. (2007). *Nanoletters*, **7**, 1138–1143.
Kolb, U., Gorelik, T., Kuebel, C., Otten, M. T. & Hubert, D. (2007). *Ultramicroscopy*, **107**, 507–513.
Kolb, U., Gorelik, T. & Otten, M. T. (2008). *Ultramicroscopy*, **108**, 763–772.
Kolb, U., Mugnaioli, E. & Gorelik, T. (2011). *Cryst. Res. Technol.* **46**, 542–554.
Landrum, G. A., Hoffmann, R., Evers, J. & Boysen, H. (1998). *Inorg. Chem.* **37**, 5754–5763.
Li, J., Huang, F., Wang, L., Yu, S. Q., Torimoto, Y., Sadakata, M. & Li, Q. X. (2005). *Chem. Mater.* **17**, 2771–2774.
Martínez-Lope, M., Alonso, J., Retuerto, M. & Fernández-Díaz, M. (2008). *Inorg. Chem.* **47**, 2634–2640.
Merli, M., Cámara, F., Domeneghetti, C. & Tazzoli, V. (2002). *Eur. J. Mineral.* **14**, 773–783.
Miyasaka, S., Okimoto, Y., Iwama, M. & Tokura, Y. (2003). *Phys. Rev. B*, **68**, 100406.
Mugnaioli, E., Gorelik, T. & Kolb, U. (2009). *Ultramicroscopy*, **109**, 758–765.
Neder, R. B. (1999). *Clays Clay Miner.* **47**, 487–494.
Oleynikov, P. (2011). *Cryst. Res. Technol.* **46**, 569–579.
Palatinus, L. (2011). *PETS. Program for Analysis of Electron Diffraction Data*. Institute of Physics, Prague.
Palatinus, L. & Chapuis, G. (2007). *J. Appl. Cryst.* **40**, 786–790.
Palatinus, L., Jacob, D., Cuvillier, P., Klementová, M., Sinkler, W. & Marks, L. D. (2013). *Acta Cryst.* A**69**, 171–188.
Palatinus, L., Petříček, V. & Corrêa, C. A. (2015). *Acta Cryst.* A**71**, 235–244.
Petříček, V., Dušek, M. & Palatinus, L. (2014). *Z. Kristallogr.* **229**, 345–352.
Sakakura, T., Tanaka, K., Takenaka, Y., Matsuishi, S., Hosono, H. & Kishimoto, S. (2011). *Acta Cryst.* B**67**, 193–204.
Sinkler, W., Own, C. S. & Marks, L. D. (2007). *Ultramicroscopy*, **107**, 543–550.
Smrčok, L., Tunega, D., Ramirez-Cuesta, A. J. & Scholtzová, E. (2010). *Phys. Chem. Miner.* **37**, 571–579.
Stimpfl, M., Ganguly, J. & Molin, G. (1999). *Contrib. Mineral. Petrol.* **136**, 297–309.
Stys, A., Kaiser-Bischoff, I., Boysen, H., Lerch, M., Hölzel, M. & Senyshin, A. (2006). *Z. Anorg. Allg. Chem.* **632**, 2136.

Tarantino, S. C., Domeneghetti, M. C., Carpenter, M. A., Shaw, C. J. S. & Tazzoli, V. (2002). *Eur. J. Mineral.* **14**, 525–536.
Toman, K. (1952). *Acta Cryst.* **5**, 329–331.
Vincent, R. & Midgley, P. A. (1994). *Ultramicroscopy*, **53**, 271–282.
Wan, W., Sun, J., Su, J., Hovmöller, S. & Zou, X. (2013). *J. Appl. Cryst.* **46**, 1863–1873.
Zhang, D., Oleynikov, P., Hovmöller, S. & Zou, X. (2010). *Z. Kristallogr.* **225**, 94–102.